Investigating the collinear splitting effects of boosted dark matter at neutrino detectors

J. High Energ. Phys. 2023, 68 (2023)
arXiv: 2302.09839 (accepted by PRD)

Junle Pei (IHEP, CAS)
Co-authors: Jinmian Li (Sichuan University)
Takaaki Nomura (Sichuan University)
Xiangwei Yin (ITP, CAS)
Cong Zhang (Sichuan University)

Axion 2023

July 24, 2023

Motivations

- Direct detection experiments are most sensitive to halo dark matter (DM) when its mass is comparable to the target. However, their sensitivity decreases rapidly for DM masses below the GeV scale.
- In astrophysics, halo DM can be boosted through various mechanisms, such as up-scattering by high-energy cosmic ray (CR) particles. This process generates a significant flux of boosted DM, detectable in direct detection and large-volume neutrino experiments installed deep underground, even for DM masses below 1 GeV.
- In neutrino detectors, the energy scale of DM-SM particle scattering typically exceeds the mass scale of the DM sector. This hierarchy results in the presence of large logarithms, making significant contributions to the differential cross section of DM scattering in terms of DM parton distribution functions (PDFs).

The simplified model and DM PDFs

Interaction between Dirac fermion DM χ ($\bar{\chi}$) and dark photon A':

$$\mathcal{L} \supset g' A'_\mu \bar{\chi}\gamma^\mu \chi \qquad (1)$$

Splitting function:

$$\frac{d\mathcal{P}_{A\to B+C}}{dz dk_T^2} \simeq \frac{1}{N}\frac{1}{16\pi^2}\frac{z\bar{z}\left|M_{\rm split}\right|^2}{\left(k_T^2+\bar{z}m_B^2+zm_C^2-z\bar{z}m_A^2\right)^2} \qquad (2)$$

$A \to B + C$	$\frac{d\mathcal{P}_{A\to B+C}}{dzdk_T^2} = P_{A\to B+C}(z)$
$\chi/\bar{\chi} \to A'_T + \chi/\bar{\chi}$	$\frac{\alpha'}{2\pi}k_T^2\frac{\frac{1+\bar{z}^2}{z}-\frac{\bar{z}}{z}\frac{2m_\chi^2z^2+m_{A'}^2\left(1+\bar{z}^2\right)}{k_T^2+m_\chi^2z^2+m_{A'}^2\bar{z}}}{k_T^2+m_\chi^2z^2+m_{A'}^2\bar{z}}$
$\chi/\bar{\chi} \to A'_L + \chi/\bar{\chi}$	$\frac{\alpha'}{\pi}k_T^2\frac{m_{A'}^2\bar{z}^2}{z\left(k_T^2+m_\chi^2z^2+m_{A'}^2\bar{z}\right)^2}$
$A'_T \to \bar{\chi}/\chi + \chi/\bar{\chi}$	$\frac{\alpha'}{2\pi}k_T^2\frac{z^2+\bar{z}^2+\frac{z\bar{z}\left(2m_\chi^2+m_{A'}^2\left(z^2+\bar{z}^2\right)\right)}{k_T^2+m_\chi^2-m_{A'}^2z\bar{z}}}{k_T^2+m_\chi^2-m_{A'}^2z\bar{z}}$
$A'_L \to \bar{\chi}/\chi + \chi/\bar{\chi}$	$\frac{2\alpha'}{\pi}k_T^2\frac{m_{A'}^2z^2\bar{z}^2}{\left(k_T^2+m_\chi^2-m_{A'}^2z\bar{z}\right)^2}$

Table 1: Splitting functions involving χ, $\bar{\chi}$, and A'.

DGLAP equations of PDFs:

$$\frac{df_i(k_T, x)}{d\ln k_T^2} = \sum_{m,n} N \int_x^1 \frac{dz}{z} P_{m\to i+n}(z) f_m\left(k_T, \frac{x}{z}\right) - \sum_{j,k} \int_0^1 dz P_{i\to j+k}(z) f_i(k_T, x) \quad (3)$$

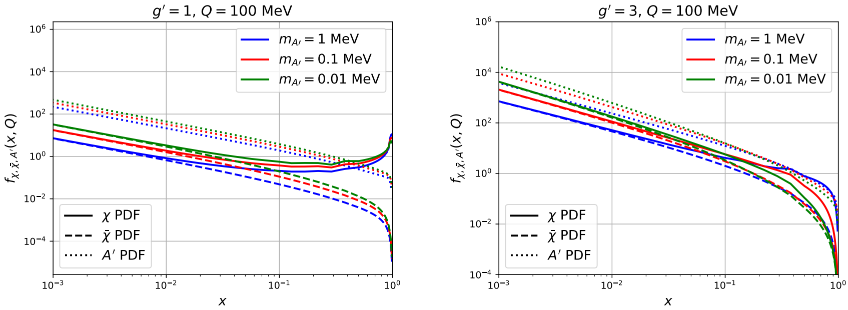

Figure 1: The PDFs of χ (solid line), $\bar{\chi}$ (dashed line) and A' (dotted line) at factorization scale of 100 MeV. Different colors indicate the dark photon mass as shown in the legend. The coupling $g' = 1$ in left panel and $g' = 3$ in right panel. The dark matter mass is taken to be 0.01 MeV. [arXiv: 2209.10816]

Boosted dark matter from cosmic ray acceleration

Electron-philic interaction:

$$\mathcal{L} \supset \epsilon \times g_{\rm em} A'_\mu \bar{e} \gamma^\mu e \tag{4}$$

DM scattered by energetic cosmic ray (CR):

$$\frac{d\sigma_{\chi e}}{dT_\chi} = g'^2 \left(\epsilon g_{\rm em}\right)^2 \frac{2m_\chi \left(m_e + T_{\rm CR}\right)^2 - T_\chi \left(\left(m_e + m_\chi\right)^2 + 2m_\chi T_{\rm CR}\right) + m_\chi T_\chi^2}{4\pi \left(2m_e T_{\rm CR} + T_{\rm CR}^2\right) \left(2m_\chi T_\chi + m_A^2\right)^2} \tag{5}$$

The recoil flux of CR-induced DM (CRDM):

$$\frac{d\Phi_\chi}{dT_\chi} = D_{\rm eff} \frac{\rho_\chi^{\rm local}}{m_\chi} \int_{T_{\rm CR}^{\rm min}}^{\infty} dT_{\rm CR} \frac{d\Phi_e}{dT_{\rm CR}} \frac{d\sigma_{\chi e}}{dT_\chi} \tag{6}$$

Boosted dark matter from cosmic ray acceleration

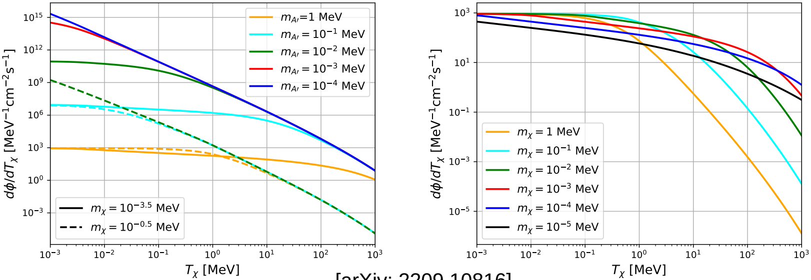

[arXiv: 2209.10816]

Figure 2: Differential CRDM flux for different DM and dark photon masses. The masses are indicated by colors and line types as explained in the legends. In the right panel, $m_{A'} = 1$ MeV is chosen. For both panels, we have chosen $g' = 1$ and $\epsilon = 1$.

Signal rate at DM direct detection experiments

A boosted CRDM scattering off an electron in target atom:

$$\chi(p_1) + e^-(p_2) \to \chi(k_1) + e^-(k_2) \tag{7}$$

The differential cross section with respect to the electron recoil kinetic energy T_R:

$$\begin{aligned}\frac{d\sigma_{nl}}{d\ln T_R} =& \frac{2l+1}{16\cdot(2\pi)^5}\frac{T_R\,|\mathbf{p_2}|}{E_\chi\left(m_e - E_B^{nl}\right)|\mathbf{p_1}|}\left|iM(p_1, p_2, k_1, k_2)\right|^2 \\ &\times \left|\chi_{nl}(|\mathbf{p_2}|)\right|^2 d\phi_{p_2}\, d|\mathbf{p_2}|\, dq\end{aligned} \tag{8}$$

The ionization rate:

$$\frac{dR_{ion}}{d\ln T_R} = \sum_{nl} N_T \int dT_\chi \frac{d\sigma_{nl}}{d\ln T_R}\frac{d\phi_\chi}{dT_\chi} \tag{9}$$

Signal rate at Neutrino detector: higher threshold

- Considering the DM PDFs becomes necessary as we primarily focus on a parameter region where the masses of DM and dark photon are significantly smaller than the typical energy scale of DM-electron scattering in neutrino detectors.
- The index i in the PDF runs over χ, $\bar{\chi}$, and A', corresponding to the scattering processes $\chi + e^- \to \chi + e^-$, $\bar{\chi} + e^- \to \bar{\chi} + e^-$, and $A' + e^- \to \gamma + e^-$, respectively.
- The ionization rate:

$$\frac{dR_{ion}}{d\ln T_R} = N_T^{SK} \sum_i \int dT_\chi^0 \int_0^{x_{\max}} dx \frac{d\sigma^i}{d\ln T_R} f_i(Q,x) \frac{d\phi_\chi}{dT_\chi^0} \Theta(xE_\chi^0 - E_i^{\min}) + N_T^{SK} \int dT_\chi \frac{d\sigma_\chi}{d\ln T_R} \frac{d\phi_\chi}{dT_\chi} \Theta(T_\chi - T_\chi^{\min}) \int_{x_{\max}}^1 f_\chi(Q,x) \tag{10}$$

Signal rate at Neutrino detector: dark Compton scattering

Dark Compton scattering:

$$A' + e^- \to \gamma + e^- \tag{11}$$

The corresponding recoil rate:

$$\frac{dR}{d\ln E_\gamma} = N_T^{SK} \int dT_\chi^0 \int_0^{x_{\max}} dx \frac{d\sigma^{A'}}{d\ln E_\gamma} f_{A'}(Q, x) \frac{d\phi_\chi}{dT_\chi^0} \times \Theta(xE_\chi^0 - E_{A'\gamma}^{\min}) \Theta(E_{A'\gamma}^{\max} - xE_\chi^0) \tag{12}$$

Results: bounds from XENON1T

- For XENON1T experiment,

$$\chi^2 = \sum_i \frac{\left[\left(\frac{dR_{\chi+B_0}}{dT_R}\right)_i - \left(\frac{dR_{obs}}{dT_R}\right)_i\right]^2}{\sigma_i^2} \; . \tag{13}$$

- The χ^2 value for background only:

$$\chi^2_{B_0} = \sum_i \frac{\left[\left(\frac{dR_{B_0}}{dT_R}\right)_i - \left(\frac{dR_{obs}}{dT_R}\right)_i\right]^2}{\sigma_i^2} = 46.4 \tag{14}$$

- Assuming the test statistic follows a χ^2 distribution with two degrees of freedom, the 2σ bound corresponds to

$$\Delta\chi^2 = \chi^2 - \chi^2_{B_0} = 6.18 \; . \tag{15}$$

Results: bounds from SuperK

- Using the Super-K experiment data corresponding to 161.9 kiloton-year exposure, the total measured number of events $N_{\rm sk}$ is 4042 in the bin $0.1 < T_e/\text{GeV} < 1.33$.
- A conservative upper limit on DM signal can be obtained by requiring

$$\xi \times N_{\rm DM} < N_{\rm sk} \ , \tag{16}$$

where the signal efficiency $\xi = 0.93$.

- $N_{\rm DM}$ is calculated by integrating $\frac{dR_{ion}}{dT_R}$ over the region $T_R > 100\ {\rm MeV}$, with total number of electrons inside the Super-K detector $N_e = 7.5 \times 10^{33}$ and data-taking period of 2628.1 days.

Results: bounds from XENON1T and SuperK

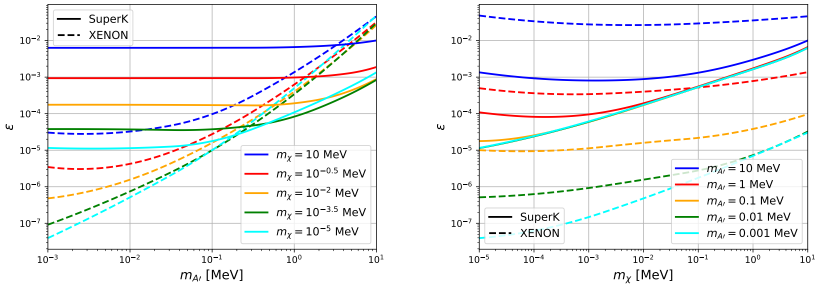

Figure 3: Left panel: exclusion limits of XENON1T (dashed lines) and Super-K (solid lines) in the $m_{A'} - \epsilon$ plane. The values of m_χ are indicated by the line colors. Right panel: exclusion limits of XENON1T (dashed lines) and Super-K (solid lines) in the $m_\chi - \epsilon$ plane. The values of $m_{A'}$ are indicated by the line colors. In both cases, the DM coupling $g' = 1$. [arXiv: 2209.10816]

Bounds from SuperK: the PDF effects

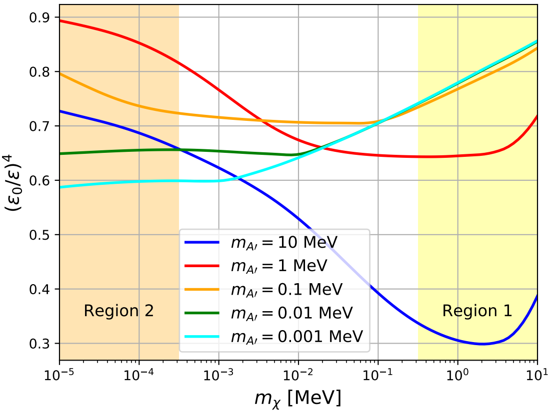

[arXiv: 2209.10816]

Figure 4: The ratio between the exclusion limits of Super-K with (denoted by ϵ) and without (denoted by ϵ_0) considering the PDF effects. The ratios for different dark photon masses are indicated by the line colors. The dark matter coupling $g' = 1$.

The PDF effects: photon signal at SuperK

The Super-K is a water-based Cherenkov detector in which the Cherenkov rings produced by photons and electrons exhibit similarities. It is challenging to distinguish a mono-energetic photon with a threshold of $\mathcal{O}(1) \sim \mathcal{O}(10)$ MeV.

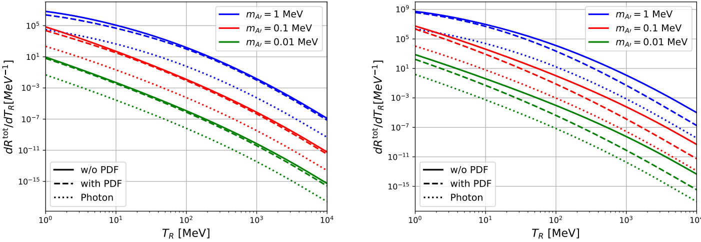

Figure 6: The differential recoil rate (at Super-K with data taking of 2628.1 days) for recoiled electron without DM PDF effects (solid line), with DM PDF effects (dashed line) and for the outgoing photon (dotted line), where we have taken fixed dark photon mass as indicated in the legend, DM mass $m_\chi = 0.01$ MeV, signal efficiency $\xi = 0.93$ and the ϵ is chosen as the maximal value that satisfies the XENON1T and Super-K bounds. Left panel: DM coupling $g' = 1$; Right panel: DM coupling $g' = 3$. [arXiv: 2209.10816]

Photon signal at DUNE and JUNO

- The DUNE and JUNO detectors possess high-efficiency photon identification capabilities, allowing for the identification of mono-energetic photons at significantly lower thresholds.
- In these detectors, an energetic single photon signal can be considered background-free, implying that even a few events can lead to exclusion or discovery.

Projected bounds from DUNE and JUNO

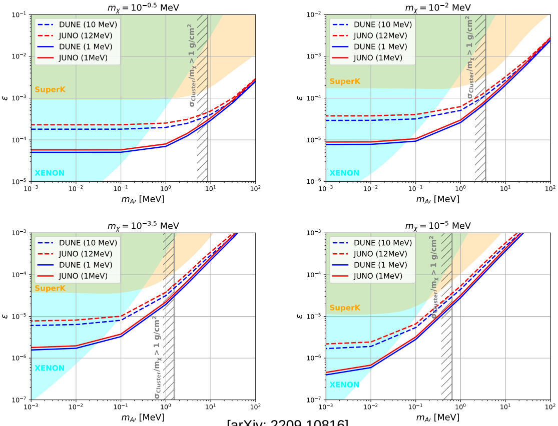

[arXiv: 2209.10816]

Figure 7: The orange shaded regions and cyan shaded regions correspond to the Super-K and XENON1T bounds. The DM self-interaction constraints are shown by hatched vertical lines, and regions on the left-hand side are excluded. The blue lines and red lines correspond to the contours of three signal photon events in each year at DUNE and JUNO, respectively. The threshold of the photon detection is indicated by the line types as explained in the legend. We choose four different DM masses for demonstration, the values of which are given in the titles of plots.

Boosting indirect detection of secluded dark matter sector

arXiv: 2302.09839

- The hidden sector interacts with the SM through portal interactions that are suppressed, allowing it to evade direct detection of dark matter (DM) and collider searches. This scenario is referred to as the secluded DM model.
- In simplified two-component DM models, the heavier DM component, which dominates the relic density, annihilates into lighter species that are boosted.
- We investigate the effects of dark showering for DM indirect detection in simplified two-component DM models with vector and pseudoscalar portal interactions.

Vector portal model

- In this case we introduce a hidden local $U(1)_H$ symmetry and SM singlet field contents

$$\text{Dirac fermions: } \chi\ (Q_\chi),\ \psi(Q_\psi), \quad \text{Scalar: } \varphi(2)\ , \tag{17}$$

requiring $|Q_\chi| \neq |Q_\psi|$, $|2Q_\chi| \neq 2$, $|2Q_\psi| \neq 2$ and $|Q_\chi \pm Q_\psi| \neq 2$.

- The relevant Lagrangian for the Dirac fermions is

$$\bar{\chi}(i\not{D} - m_\chi)\chi + \bar{\psi}(i\not{D} - m_\psi)\psi, \tag{18}$$

where $D_\mu\chi(\psi) = (\partial_\mu + iQ_{\chi(\psi)}g_H Z'_\mu)\chi(\psi)$ is the covariant derivative with g_H being gauge coupling of $U(1)_H$.

Pseudo-scalar portal model

- In this case we introduce a hidden global $U(1)'_H \times Z_2^A \times Z_2^B$ symmetry where $U(1)'_H$ is softly broken, and field contents are

$$\begin{aligned} \text{Fermions}: \ & \chi_L(0,+,-), \ \chi_R(Q,+,-), \\ & \psi_L(0,-,+), \ \psi_R(Q,-,+), \\ \text{Scalar}: \ & \varphi'(-Q,+,+). \end{aligned} \tag{19}$$

- Pseudo-scalar portal interactions

$$\begin{aligned} \mathcal{L} \supset & \ y_\chi \overline{\chi_L} \chi_R \varphi' + y_\psi \overline{\psi_L} \psi_R \varphi' + h.c. \\ \supset & \ iA(y_{A\chi\chi} \bar{\chi} \gamma_5 \chi + y_{A\psi\psi} \bar{\psi} \gamma_5 \psi), \end{aligned} \tag{20}$$

where $\varphi' = (\phi + iA)/\sqrt{2}$ and $y_{A\chi\chi(A\psi\psi)} \equiv y_{\chi(\psi)}/\sqrt{2}$.

Dark parton shower

Sudakov form factor:

$$\Delta_a\left(Q_{\max};Q_{\min}\right)=\exp\left[-\sum_{bc}\int_{\ln Q^2_{\min}}^{\ln Q^2_{\max}} d\ln Q^2\int_{z_{\min}(Q)}^{z_{\max}(Q)} dz\frac{d\mathcal{P}_{a\to b+c}(z,Q)}{dz\,d\ln Q^2}\right] \quad (21)$$

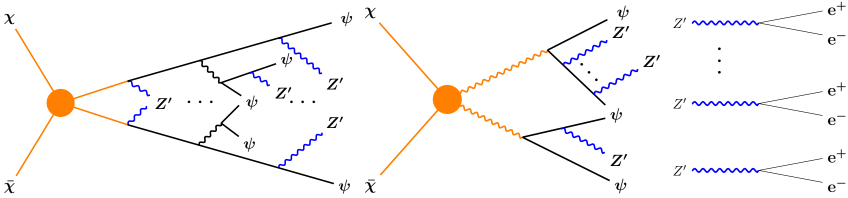

FIG. 1. Indirect detection signature for $\chi\chi$ annihilation in the vector portal model. [arXiv: 2302.09839]

Signal rate

- In pseudo-scalar portal model, the differential flux of gamma-rays at the location of the earth is

$$\frac{d\Phi_\gamma}{dE_\gamma} = \frac{1}{\eta}\frac{1}{4\pi}\frac{1}{m_\chi^2} J \sum_{f=\psi,A} \langle\sigma_A v\rangle_f \frac{dN_\gamma^f}{dE_\gamma} \ . \tag{22}$$

- In vector portal model, the differential flux of positron at the location of the earth can be calculated by convoluting the spectra at production with the propagation functions:

$$\begin{aligned}\frac{d\Phi_{e^+}}{dE_{e^+}}(E) =& \frac{v_{e^+}}{4\pi b(E, r_{\rm sun})}\frac{1}{\eta}\left(\frac{\rho(r_{\rm sun})}{m_\chi}\right)^2 \\ &\times \sum_{f=\psi,Z'} \langle\sigma v\rangle_f \int_E^{m_\chi} dE_{\rm s} \frac{dN_{e^+}^f}{dE}(E_{\rm s})\, I(E, E_{\rm s}, r_{\rm sun})\end{aligned} \tag{23}$$

Results: bounds from Fermi-LAT and AMS-02

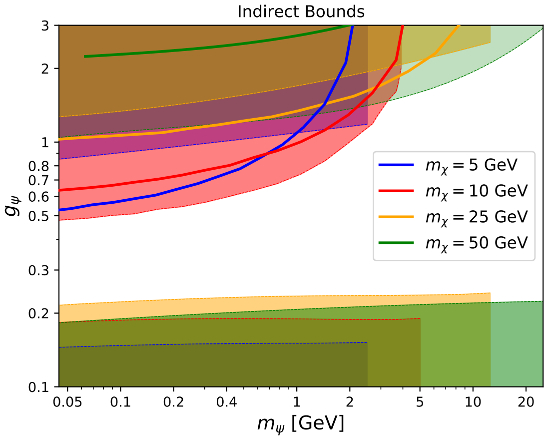

FIG. 2. Indirect detection bounds from Fermi-LAT for pseudoscalar portal model (solid line) and from AMS-02 for vector portal model (shaded region). [arXiv: 2302.09839]

Summary

- In the simplified electron-philic dark photon model with fermionic DM, we find that in the parameter space with a heavy dark photon and light DM, the spectrum of CRDM flux is flatter, which means that DM particles with energies well above the detector threshold can contribute significantly to DM-electron scattering.
- The XENON1T detector's low energy threshold is highly sensitive to the parameter space with a light $m_{A'}$, effectively ruling out small couplings ϵ as low as 10^{-7}.
- The high-energy electron recoil signals observed at neutrino detectors can be generated by DM, anti-DM, and dark photon components in the DM PDFs. Interestingly, our findings suggest that these PDF effects reduce the electron recoil rate at neutrino detectors, thus alleviating the associated constraints.
- The presence of a dark photon component in the DM PDFs can lead to dark Compton scattering, a phenomenon that can be effectively investigated in upcoming neutrino detectors like DUNE and JUNO.
- We study the dark showering effects in simplified two-component dark matter models with vector and pseudoscalar portal interactions for indirect detection. Considering constraints from AMS-02 positron data and Fermi-LAT gamma-ray measurements of dwarf galaxies, we find that the dark showering phenomenon reveals a previously unexplored sensitive region.